

Investigation of the Concentric Heat Pump with Improved Energy Performance

Demessova Saule¹, Omarov Rashit², Ivaylo Stoyanov³, Omar Dauren²,
Yerzhigitov Yerkin¹, Abdygaliyeva Slushash⁴

¹ Kazakh National Agrarian University, Almaty 050000, Kazakhstan

² Scientific production center of agricultural center LLP, Almaty 050005, Kazakhstan

³ University of Ruse, 8 Studentska Str., 7017 Ruse, Bulgaria

⁴ Al-Farabi Kazakh National University, Almaty 050040, Kazakhstan

Abstract – This paper investigates the energy characteristics of the concentric heat pump. The heat exchanger of the evaporator of the "pipe in pipe" type, through the inner copper tube of which the refrigerant circulates, and inside the outer pipe - the coolant, is placed in a spiral around the compressor, cooling it and at the same time absorbing the heat released by it. The new design improves technical and economic performance. Experimental results were carried out, which confirm the possibility of maintaining the compressor temperature (80-90°C), increasing the heat output and conversion coefficient (COP) by an average of 10-15%. The proposed technical solution makes it possible to improve the energy efficiency of the concentric heat pump due to the absorption of the excess heat from the evaporator in the general heat flow and to reduce the emissions of CO₂.

Keywords – Heat pump, energy efficiency, low potential heat source.

1. Introduction

In many industries, the goal is to increase the efficiency of heating the environment or equipment under severe conditions.

DOI: 10.18421/TEM124-53

<https://doi.org/10.18421/TEM124-53>


Corresponding author: Ivaylo Stoyanov,
University of Ruse, Department of Electrical Power
Engineering, 8 Studentska Str., 7017 Ruse, Bulgaria
Email: stoyanov@uni-ruse.bg

Received: 20 July 2023.

Revised: 21 September 2023.

Accepted: 06 October 2023.

Published: 27 November 2023.

 © 2023 Demessova Saule et al; published by UIKTEN. This work is licensed under the Creative Commons Attribution-NonCommercial-NoDerivs 4.0 License.

The article is published with Open Access at <https://www.temjournal.com/>

Different options include installing built-in or mobile heaters, infrared emitters, steam generators, and heat pumps (HP) [1]. An energy consumption analysis accompanied by an economic evaluation is always necessary to select an option.

The HP is widely used in heating and cooling systems for buildings and production processes [2], [3], [4]. Energy saving and energy efficiency are achieved through the use of low-quality heat sources (LHP), including RES (wastewater, water bodies, atmospheric air) [5]. A comparative study of a conventional gas boiler with an environmentally friendly heating system from HP, which confirmed energy consumption savings and a reduction in annual operating costs (LCC) of 26.4% or \$48,000 was conducted in the study [6]. Various schemes for using HP are known. For example, installing an HP condenser in the exhaust pipe of liquid fuel hot water boilers to recover the condensation latent heat of low-temperature water vapour from the flue gases, which also reduces the emissions of CO₂ contained in the flue gases [7]. Other researchers investigated the use of HP to recover waste heat at 45°C to generate steam above 150°C. For combined HP with much higher efficiency, with the lowest installation cost for pellets and diesel fuel with boiler, they are approximately 30% smaller than those of a gas boiler system and about 60% of an HP system [8]. In this way, higher efficiency is obtained and the performance of HP systems is improved [9]. A prototype HP heating system for using ground heat in a harsh continental climate has been developed and tested at Al-Farabi Kazakh National University [10].

HP served as the basis for the creation of hybrid or integrated systems, which are also called polyvalent, in which, unlike monovalent, the heat of several NPIs is used. An environmental factor in which the use of biomass energy as an additional NPI reduced CO₂ emissions by 54.1% [11]. An integrated system that uses the heat contained in the air of the livestock building, chilled milk, heat from solar energy and atmospheric air was suggested for use in [12].

At the same time, the air in the room is cleaned of excess moisture and gases formed during the life of the animals [12]. The hybrid system consisting of a photovoltaic plant (PV), solar concentrator (PV/T), HP, and absorption chiller (AC), provides stable heating and air conditioning of the building. The system energy efficiency is 32.98%, exergy efficiency is 17.62%, payback period (PP) is 7.77 years as suggested in [13]. The cogeneration system generates electricity and heat for heating. The solar energy is supplied to the solar power plant by a concentrator solar power plant (CPVT), and the HP evaporator is used to cool the solar plant after implementation, the efficiency of CPVT increases by 4% [14]. A SWOT analysis is offered for easy selection of types of energy sources for constructing a polyvalent system [8]. Researchers from China have proposed a new type of hybrid compression-absorption heat pump, in which compared with traditional radiator cycles, the temperature is increased to 200°C and COP to 3.249, with very satisfactory performance of the evaporator and condenser [15]. The investigated system consists of 3 air-to-water HVAC units, 1 water storage tank, and 1 fan coil unit (FCUs) for cooling and heating; a three-section greenhouse under local climate conditions confirmed stable heating but insufficient cooling [16]. A new absorption HP $\text{H}_2\text{O}/\text{LiBr}$ with heat recovery for combined heating and cooling was proposed in [17]. The energy optima of a heating system with HP are considered [18]. The authors have developed a multi-objective optimization procedure that allows you to choose the engine power pumps to achieve maximum efficiency.

Due to environmental factors, carbon dioxide is widely studied as an alternative refrigerant. In a novel thermoelectric sub-cooler-expander with transcritical CO_2 and a thermoelectric sub-cooler, the system efficiency (COP_h and COP) before and after the application was 4.19% and 4.62%, respectively [19]. As a result of the search for an environmentally friendly alternative to R134a, it was found that R152a is one alternative to R134a on COP_{cycle}, COP_{system} with calculated values of 3.09, 2.91, which amounts to 31.76 tons of CO_2 equivalent. The refrigerants R1234yf and R1234ze have been identified as intermediate substitutes for R134a. Some authors recommended the use of R1336mzz (E) as an alternative to R134a, but the main problem is the internal heat exchanger. Liquid CO_2 (transcritical CO_2) refrigerants are being researched for electric vehicle thermal control systems, internal cooling/heating, and fast battery charging of electric vehicles [21], [22].

In general, efficiency gains are achieved by improving the main HP components where compressors have the greatest potential [23], [24], [25]. Some authors recommended using DC motors to enable adaptive control of their speed [26], [27].

Others suggest using spiral compressors with inverter control of the flow of the refrigerant (VFR variable flow refrigerant), in which the engine temperature is up to 120°, the temperature of the suction steam is 145÷155 °C, and the temperature of the compressed steam is 170÷190°C [28]. Overheating of the motor windings above 130°C is undesirable. The HP Mitsubishi Electric ZUBADAN uses two-phase refrigeration with refrigerant injection into the compressor. The cooling is done by evaporating the pre-condenser freon to the coil which is located in the compressor oil bath [30], where the temperature of the electric motor has decreased by 15÷ 20 °C [31]. An electronic cooling system CIC (System, i.e. Controlled Injection Cooling) is known [32].

For a long time, HP used metal-intensive and expensive plate heat exchangers of the Swedish company Alfa Laval, made of stainless steel. A tube-in-tube heat exchanger where refrigerant (CO_2) circulates through the inner copper tubes and water (H_2O) circulates through the annulus is proposed in [32]. In the evaporator the heat flow is from the water to the refrigerant and in the condenser, the water takes heat from the heated refrigerant. One possibility to increase the heat exchange is to divide the inner tubes into three parallel tubes (branches). The heat exchange between the exchange working bodies takes place directly through the thin walls of the copper pipes; copper pipes, unlike plate heat exchangers, are designed for higher pressure; the production of such heat exchangers does not require special machines and complex technological equipment.

A similar construction was proposed by the authors of this paper [33], [34]. The main difference is the construction of the condenser and evaporator piping. The heat exchangers consist of tube-in-tube coils with the same diameter and coil pitch, arranged in a spiral configuration with a minimum spacing between them. Refrigerant circulates through the internal copper pipes and water or antifreeze (in the evaporator) circulates in the annular space where the copper pipes are laid in a spiral to create a rotary circulation of the coolant. Laying the evaporator tube concentrically around the compressor provides cooling of the compressor by absorbing the heat generated by the evaporator.

2. Research Methodology

Figure 1 shows the structural and process diagram of the studied HP. The tube heat exchanger is made of the "tube-in-tube" type, through which the refrigerant (CO_2) circulates inside the copper tube, and water (H_2O) circulates between the tubes. Laying the heat exchanger of the tubular evaporator in a spiral around the compressor provides protection for the compressor from overheating and self-regulating maintenance of its temperature regime.

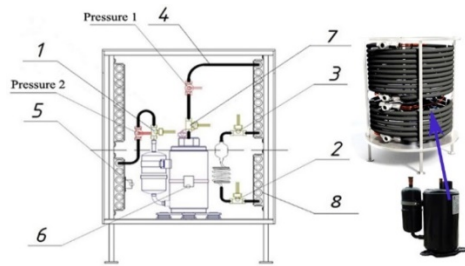


Figure 1. Structural scheme of the proposed HP: temperature sensors 1 and 2 - outlet and inlet of the refrigerant evaporator; 3 and 4 - outlet and inlet condenser refrigerant; 5 - the environment; 6 - side surface, 7 - compressor head, 8 - heat exchange tubes

The sensors "pressure-1" and "pressure-2" indicate the pressure of the refrigerant at the compressor outlet and inlet.

The compressor heating equation can be considered as the process of heating the body from an internal heat source, with a constant power P.

$$P \cdot \partial\tau = C \cdot \partial t + k_{\tau 0} \cdot S \cdot \partial\tau. \quad (1)$$

After appropriate transformations, equation (1) reduces to the form:

$$\frac{\partial t}{\partial \tau} + \frac{k_{\tau 0} \cdot S}{C} \cdot t - \frac{P}{C} = 0. \quad (2)$$

The solution of equation (2) is the dependence:

$$t = t_i + t_2 = \frac{P}{k_{\tau 0} \cdot S} + A \cdot e^{\frac{\tau}{T}}. \quad (3)$$

Taking into account that at $\tau = 0$ and $t=0$ and we made transformations, we get:

$$t = \frac{P}{k_{\tau 0} \cdot S} + (1 - e^{-\tau/T}).$$

The general solution of equation (2) will be:

$$t = t_{est} \cdot e^{-\frac{\tau}{T}} + \frac{P}{k_{\tau 0} \cdot S} \cdot (1 - e^{-\tau/T}); \quad (4)$$

$$t = t_{beg} \cdot e^{-\frac{\tau}{T}} + t_{est} \cdot (1 - e^{-\tau/T}). \quad (5)$$

where $\tau = \infty$; $t = t_{est}$.

The scheme of the experimental research information system is shown in Figure 2.

The basis of the information system is a controller, a server, and a personal computer with software.

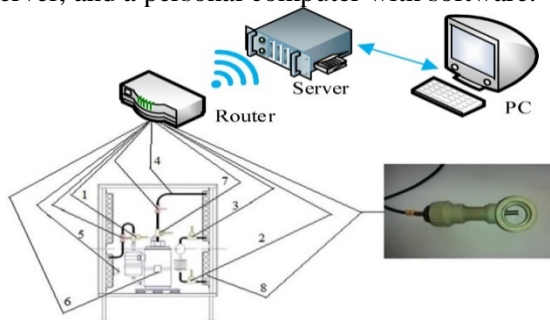


Figure 2. General schematic of the experimental installation

A schematic diagram of the controller with a connection of 8 temperature sensors DS18B20, 2 sensors for pressure WikaR1W2B30 and 2 sensors for flow G1WFM and implementation of the defined action algorithm (Figure 3).

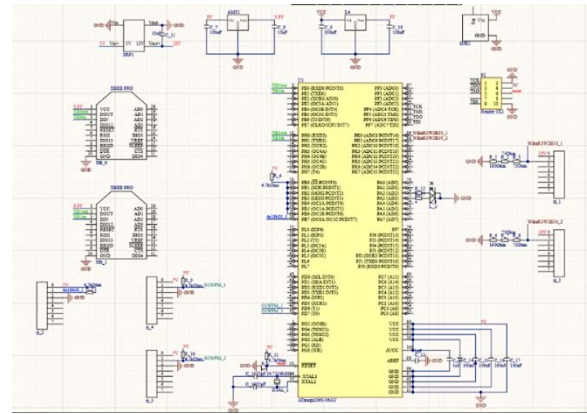


Figure 3. Controller schematic diagram

The main element of the scheme is the Atmega2560 controller, which polls and receives data from all sensors in parallel from different inputs. It should be noted that all temperature sensors are connected through one input PB7. This capability is due to the fact that the DS18B20 is originally digital and operates on the OneWire protocol, which in turn allows all DS18B20 sensors to be on one bus and work stably. This feature greatly simplifies the circuit. In the case of pressure and flow sensors, this is not possible, and therefore each sensor is connected to a separate input: PK0, PK1 - for pressure sensors, PD6, PD7 - for flow sensors.

The received data do not need initial processing and are stored in the controller's memory in the same form. The DS18B20 wiring diagram is shown below in Figure 4.

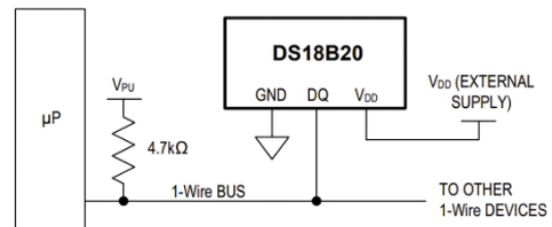


Figure 4. DS18B20 wiring diagram

In the circuit diagram, the temperature sensor is connected according to the OneWire manual [35]. Resistor R_9 plays the role of "pullup" to ensure a stable potential of the common bus. The pressure sensors generate an analogue signal, which is then processed by the controller's ADC and converted into digitized data. Resistors R_1, R_2, and R_3 are added as an extra load to prevent high currents according to the WikaR1 user manual [36]. Flow sensors generate pulses during rotation of the axis of rotation, which are read by a special counter (timer). Knowing the number of pulses per unit time, it is possible to calculate the volume of water that passes through the section. These calculations are also done in the controller. Resistors R_9 and R_10 are used to create potential on the signal wire.

The pulses appear when the flowmeter "presses" the signal wire to "ground". In addition, the processed data is formed into a packet and transmitted to the XBEE transceiver via input/output PE0 and PE1 using the UART protocol. Once in XBEE, this packet is transmitted to the server via the ZigBee protocol for further processing and storage. Stabilizer L4 with capacitors C_9 and C_10 are used to convert and stabilize the input voltage (5V - 12V) in order to provide additional power to the entire circuit. The AMS1 element with capacitors C_7 and C_8 respectively converts 5V to 3.3V and is used to power the XBEE modules. The SPR1 and C_11 elements step up the voltage from 5V to 12V to power the WikaR1 pressure sensors. The remaining elements in the circuit are used to stabilize the operation of the entire circuit under different environmental conditions according to the Atmega2560 manual [37].

The data collection process initiates the central unit. The registration of the measured data is carried out by the sensors, which convert the measured values into electrical signals. With the help of the modules, the data is converted into a suitable form and sent to the server. In it, the data received are processed and stored in a database.

3. Analysis of Research Results

An overview of the graphs (Figure 5) of the distribution of the temperature fields of the studied HP with 3 variants of the mutual location of the compressor (CP) and evaporator (EVP) shows the influence of the mutual location of the CP and EVP on the heat exchange processes of the studied HP.

3.1. HP Compressor Temperature Analysis

Figure 6 shows the comparative composite graphs of the compressor temperature for 3 variants of the gearbox placement inside the evaporator. The recording is done using sensor 6 attached to the compressors (Figure 2).

Overall, the graphs show active heat exchange between the evaporator wall and the compressor casing. This is manifested in the fact that when an insulating screen is installed between the evaporator and the compressor. It can be seen from Figure 5 that in this case, the temperature of the compressor rises to 90°C (red line). In the version with the screen removed, the temperature of the compressor reaches 80°C. That is, it decreases by 10°C.

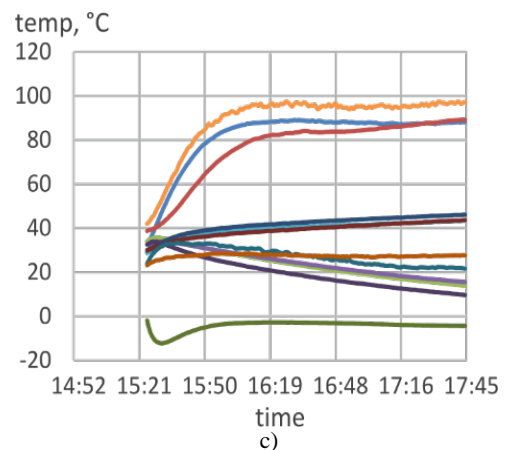
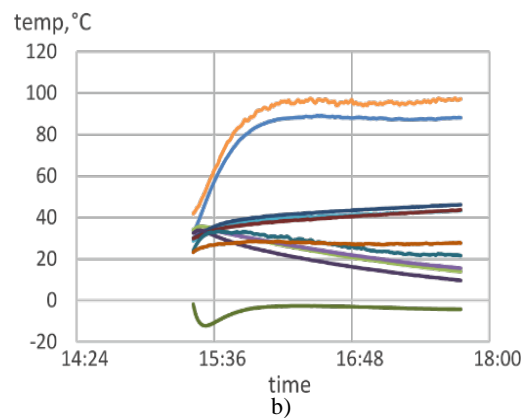
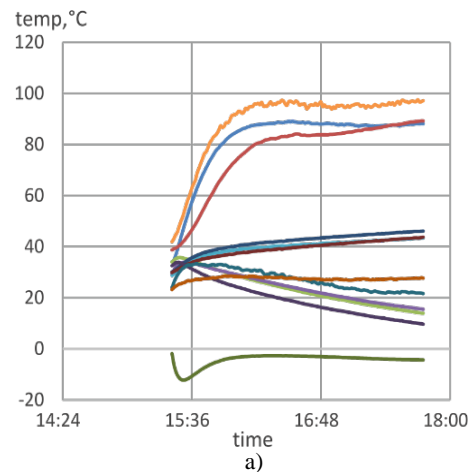


Figure 5. Distribution of the temperature fields of the HP with 3 options for the mutual location of CP and EVP: the compressor is in the centre (a), close to the wall (b), shielded from the evaporator (c)

A comparison of the bottom 2 graphs in Figure 6, when the screen is not shown, shows that over time they level off at the 80°C level. But in the initial stage, until about the 50th minute, the compressor cools better when it is not located in the centre, but near the wall of the evaporator (green line).

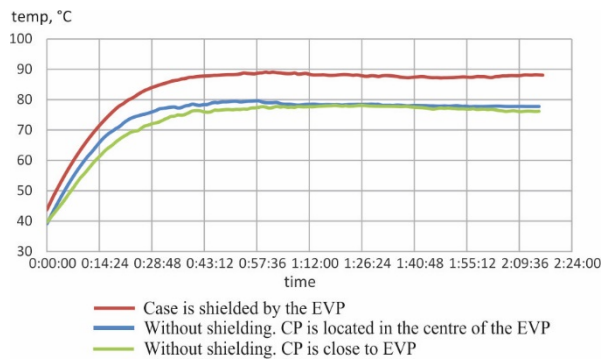


Figure 6. HP Compressor Temperature Graphs for 3 Gearbox Location Options vs EVP

3.2. HP Evaporator Refrigerant Temperature Analysis

Figure 7 shows the temperature dependences of the refrigerant (CA) at the inlet (bottom) and at the outlet of the evaporator (top), with 3 options for placing the CP inside the evaporator. The temperature is recorded at the inlet from sensor 2, at the outlet from sensor 1, embedded in the corresponding points, directly in the pipes, as shown in Figure 2.

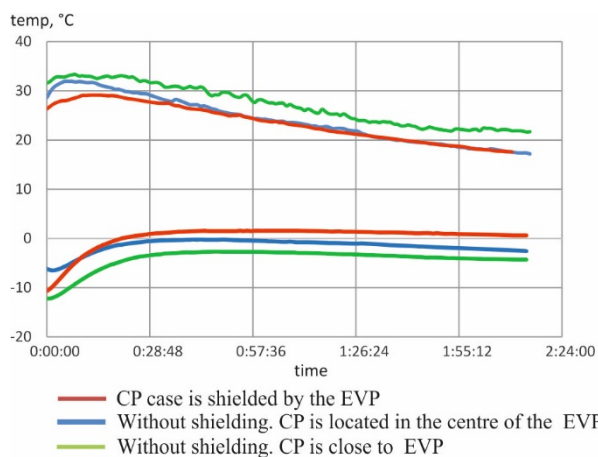


Figure 7. Refrigerant inlet (lower graphs) and evaporator outlet (upper graphs) temperature graphs, with 3 options for CP versus EVP location

We will consider these graphs from the temperature difference point XA - Δt_{1S} at the inlet and outlet of their EVP. It shows the absorption of thermal energy by CA as it passes through EVP.

As a simple visualization shows, the smallest difference is observed when shielding the CP case from the EVP. For example, when the refrigerant enters the evaporator, its temperature is approximately $+3^{\circ}\text{C}$ (red). It turns out, that EVP with a temperature of about $+30^{\circ}\text{C}$, which then decreases to $+15^{\circ}\text{C}$. The difference is changed from 27°C , at the beginning of the process. The graphs (red) are then added together and the difference is about 12°C . That is, the arithmetic mean value of the temperature difference is $\Delta t_1 = 19.5^{\circ}\text{C}$.

The biggest difference is between the green graphs (green), which show the unshielded CP temperatures when the EVP is close to the EVP. For example, when the refrigerant enters the evaporator its temperature is about -4°C (green). It exits the EVP with a temperature of about $+33^{\circ}\text{C}$, which then decreases to $+23^{\circ}\text{C}$. That is, the difference at the beginning of the process is 37°C ($+33 - (-4)$). The graphs (green) are then added and the difference is about 27°C . That is, the arithmetic mean value of the temperature difference is $\Delta t_2 = 32^{\circ}\text{C}$.

The average difference is observed between the blue graphs (blue), which show the refrigerant temperatures without shielding when the CP is located in the center of the EVP. For example, the refrigerant enters the evaporator with a temperature of about -2°C (blue). It turns out from EVP with a temperature of about $+32^{\circ}\text{C}$, which then decreases to $+23^{\circ}\text{C}$. That is, the difference at the beginning of the process is 34°C ($+32 - (-2)$). The graphs (blue) are then added and the difference is about 25°C . That is, the arithmetic mean value of the temperature difference is $\Delta t_3 = 29.5^{\circ}\text{C}$. Calculations show that the increase in heat output when the CP is not shielded is 18%.

3.3. HP Condenser Refrigerant Temperature Analysis

Figure 8 shows comparatively combined graphs of the temperatures of the refrigerant (the refrigerant) at the inlet (upper group of graphs) and the outlet of the condenser (CC) (lower group of graphs), with 3 options for the location of the condenser inside the evaporator. The temperature is recorded at the input from sensor 4, at the output from sensor 3 embedded in the corresponding points, directly in the copper pipes (Figure 2). The analysis shows, that the biggest difference is observed between the red graphs (red), which show the temperatures of the refrigerant without shielding, CP from EVP. For example, the refrigerant enters the evaporator at CC with a temperature of about $+95^{\circ}\text{C}$ (red). It turns out from COP with a temperature of about $+42^{\circ}\text{C}$. The temperature difference in the heat exchange stabilization mode is $\Delta t_2 = 53^{\circ}\text{C}$.

The temperature difference between the blue (blue) and green (green) graphs, which show the unshielded refrigerant temperatures when the CP is located in the center and close to the EVP, is almost the same, 42°C .

It follows from the graphs that in the first variant (red) additional thermal energy is added by the overheated gearbox housing. The options for placement of the CP relative to the EVP (blue) and (green) practically do not affect the effectiveness of the CP.

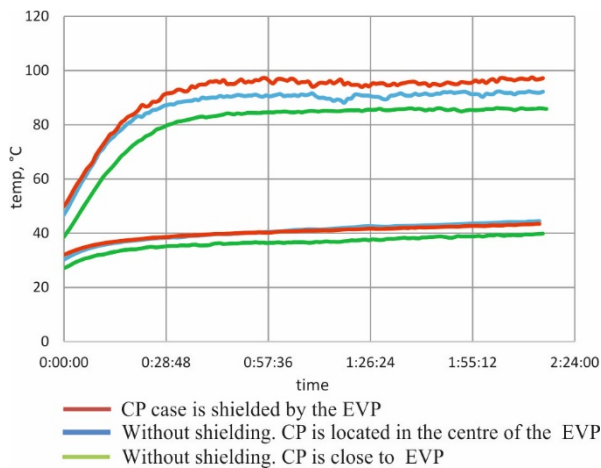


Figure 8. Refrigerant inlet (upper graphs) and condenser outlet (lower graphs) graphs

However the overheating of CC, which is observed in the variant of shielding CC from EVP, reduces the technical resources of HP, which is undesirable.

3.4. Analysis of the Air Temperature Around the CP

The graphs of the air temperature around the CP (sensor 5) and the surface of the EVP (sensor 8) are shown in Figure 9.

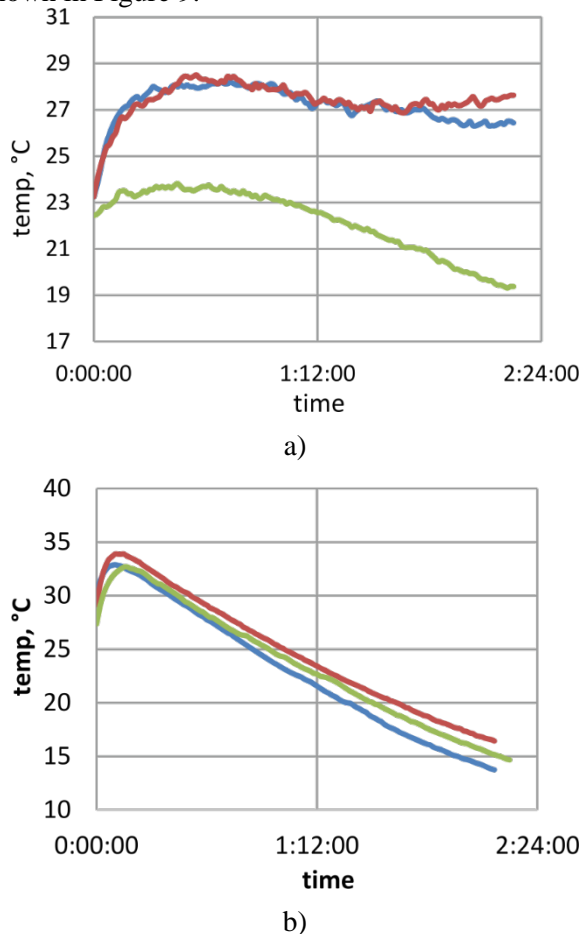


Figure 9. Dependence between the air temperature between the evaporator and the compressor: the compressor sensor (a); evaporator sensor (b)

Figure 9 shows that the air temperature around the compressor station is quite stable and normal for the operation of the compressor station. With compressor shielding, which can be considered unfavourable for the CP, the temperature does not exceed 28°C, and when the CP is installed near the EVP, it is lower by 10°C. The favourable temperature regime for the operation of the CP will help to extend the technical life of the CP. The location of the CC has no practical effect on evaporator temperature was observed (Figure 9.b), which confirms the sufficient cooling ability of the CC.

3.5. Analysis of Heating and Cooling Power HP

Graphs: heating and cooling power and compressor station power (Figure 10).

The location of CP relative to EVP affects HP performance. At the same time, the power consumption in all options is almost the same (Figure 10 a, bottom three graphs).

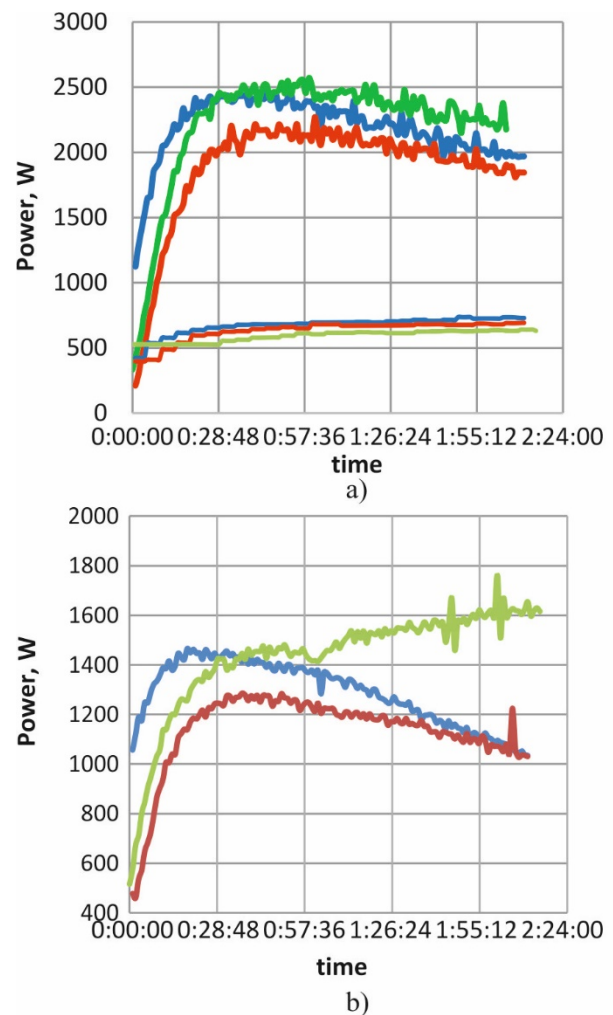


Figure 10. Heating and cooling power and HP power

As can be seen, the heat and cooling capacity increases in unshielded mode (—) when EVP is close to EVP.

This indicates an increase in the thermal energy of the emitted CP absorbed by the EVP, which complements the main flux coming from the NPI. It is observed that the temperature difference is about 60°C between the CP and EVP walls. This means that the main flow between the surfaces is radiation heat transfer. The decrease in performance in the 3rd variant (—) allows us to assume that the radiative heat exchange between CP and EVP is shielded. In general, cooling capacity curves correlate with heating capacity curves.

4. Conclusion

Based on a theoretical analysis of HP heating patterns, it was found that the degree of heating results from the balance of compressor and motor heat losses due to refrigerant gas compression, copper losses, steel losses, and heat transfer from the surface of the compressor by convection and thermal radiation.

The influence of the evaporator heat exchanger, located concentrically around the compressor, on the cooling of the compressor, without the use of a fan, on the cooling and heating characteristics of the HP, was experimentally investigated by thermodynamic analysis of individual components.

It has been experimentally confirmed that by installing an insulating screen between the walls of the evaporator and the compressor, the cooling effect of the HP compressor is improved. In case there is no screen, the compressor heats up to 80°C. In the variant where the screen blocks the direct heat exchange between the compressor and the evaporator, the compressor heats up to 90 °C.

The effect of heat absorption of the HP compressor from the evaporator is confirmed by the method of evaluating the degree of heating of the refrigerant when passing through the evaporator, by comparing the design variants studied. When the compressor casing approached the inner wall of the evaporator, the temperature difference between the refrigerant inlet and outlet of the evaporator was $\Delta t_1 = 32^\circ\text{C}$. When the compressor was installed in the center, the difference was $\Delta t_2 = 29.5^\circ\text{C}$. In the case of the isolated compressor, it is $\Delta t_3 = 19.5^\circ\text{C}$. The results show that the maximum heat absorption of the compressor is when the compressor casing comes closer to the inner wall of the evaporator, compared to the other variants.

The experimentally measured temperature regime of the condenser of HP confirms that the cooling of the compressor, which improves its operating conditions and the absorption of the heat of the evaporator compressor, increases the thermal power of the HP by 10-15% on average.

References:

- [1]. Minin, I., Nedyalkov, P., Hristova, T., Kraychev, E., & Dimov, E. (2023). Conceptual options for solving the problem of icing rollers and drums of belt conveyors. In *IOP Conference Series: Earth and Environmental Science*, 1156(1), 0012001. IOP Publishing.
- [2]. Mohamed, A. F., Gomaa, M. M., Amir, A. A., & Ragab, A. (2023). Energy, Thermal, and Economic Benefits of Aerogel Glazing Systems for Educational Buildings in Hot Arid Climates. *Sustainability*, 15(8), 6332.
- [3]. Xiao, T., & Liu, Z. (2023). Air Pollution and Enterprise Energy Efficiency: Evidence from Energy-Intensive Manufacturing Industries in China. *Sustainability*, 15(7), 6311. Doi: 10.3390/su15076311.
- [4]. Yang, L., Jia, X., & Peng, X. (2023). Analysis of the Thermodynamic Characteristics of a Hyper-Compressor through Numerical Simulation and Experimental Investigation. *Applied Sciences*, 13(7), 4478. Doi: 10.3390/app13074478.
- [5]. *Heat pump. ZUBADAN*. (n.d.) Mitsubishi Electric. Retrieved from: <http://www.mitsubishielectric.com.ua/zubadan.html>. [accessed: 21 July 2023].
- [6]. Kul, O., & Uğural, M. N. (2022). Comparative Economic and Experimental Assessment of Air Source Heat Pump and Gas-fired boiler: A Case Study from Turkey. *Sustainability*, 14(21), 14298. Doi: 10.3390/su142114298.
- [7]. Goričanec, D., Ivanovski, I., Krope, J., & Urbanc, D. (2020). The exploitation of low-temperature hot water boiler sources with high-temperature heat pump integration. *Energies*, 13(23), 6311. Doi:10.3390/en13236311
- [8]. Karadjov, M., & Hristova, T. (2023). Application of SWOT Analysis for the Selection of a Hybrid System for Heating and Production of Energy and Hot Water for the Conditions of Bulgaria. In *2023 18th Conference on Electrical Machines, Drives and Power Systems (ELMA)*, 1-4. IEEE.
- [9]. Zhang, C., Chai, D., Pan, X., Xie, J., & Chen, J. (2022). Performance Analysis of Two Systems Combining Heat Pump and Water Vapor Compression for Waste Heat Recovery. *Applied Sciences*, 12(24), 12853. Doi: 10.3390/app122412853.
- [10]. Yerdesh, Y., Amanzholov, T., Aliuly, A., Seitov, A., Toleukhanov, A., Murugesan, M., ... & Belyayev, Y. (2022). Experimental and Theoretical Investigations of a Ground Source Heat Pump System for Water and Space Heating Applications in Kazakhstan. *Energies*, 15(22), 8336. Doi: 10.3390/en15228336.
- [11]. Buday, T., & Buday-Bódi, E. (2023). Reduction in CO₂ Emissions with Bivalent Heat Pump Systems. *Energies*, 16(7), 3209. Doi: 10.3390/en16073209.

- [12]. Rashit, O., Slushash, A., Dauren, O., & Kunelbayev, M. (2017). Integrated system for the use of solar energy in the animal farm. *Scientia Iranica*, 24(6), 3213-3222.
- [13]. Yue, H., Xu, Z., Chu, S., Cheng, C., Zhang, H., Chen, H., & Ai, D. (2023). Study on the Performance of Photovoltaic/Thermal Collector–Heat Pump–Absorption Chiller Tri-Generation Supply System. *Energies*, 16(7), 3034. Doi: 10.3390/en16073034.
- [14]. Genbach A., D. Bondartsev, I. Iliev & A. Georgiev (2020). Scientific method of creation of ecologically clean capillary-porous systems of cooling of power equipment elements of power plants on the example of gas turbines, *Energy*, 199, 117458, Doi: 10.1016/j.energy.2020.117458.
- [15]. Sun, J., Wang, Y., Wu, K., Ge, Z., & Yang, Y. (2022). Analysis of a New Super High Temperature Hybrid Absorption-Compression Heat Pump Cycle. *Energies*, 15(20), 7515. Doi: 10.3390/en15207515.
- [16]. Rasheed, A., Lee, J. W., Kim, H. T., & Lee, H. W. (2022). Study on Heating and Cooling Performance of Air-to-Water Heat Pump System for Protected Horticulture. *Energies*, 15(15), 5467. Doi: 10.3390/en15155467.
- [17]. Prieto, J., Ayou, D. S., & Coronas, A. (2022). A Novel H₂O/LiBr Absorption Heat Pump with Condensation Heat Recovery for Combined Heating and Cooling Production: Energy Analysis for Different Applications. *Clean Technologies*, 5(1), 51-73. Doi: 10.3390/cleantechnol5010004.
- [18]. Nyers, A., & Nyers, J. (2023). Enhancing the Energy Efficiency—COP of the Heat Pump Heating System by Energy Optimization and a Case Study. *Energies*, 16(7), 2981. Doi: 10.3390/en16072981.
- [19]. Yang, J., Wang, L., Han, Y., Zhang, X., & Du, Y. (2022). Simulation and Experimental Study of CO₂ Transcritical Heat Pump System with Thermoelectric Subcooling. *Designs*, 6(6), 115. Doi: 10.3390/designs6060115.
- [20]. Drogenik, J., Urbanc, D., & Goričanec, D. (2022). Comparison of the New Refrigerant R1336mzz (E) with R1234ze (E) as an Alternative to R134a for Use in Heat Pumps. *Processes*, 10(2), 218. Doi: 10.3390/pr10020218.
- [21]. Wu, Z., Bi, F., Fei, J., Zheng, Z., Song, Y., & Cao, F. (2023). The Collaborative Optimization of the Discharge Pressure and Heat Recovery Rate in a Transcritical CO₂ Heat Pump Used in Extremely Low Temperature Environment. *Energies*, 16(4), 2059. Doi: 10.3390/en16042059
- [22]. Wang, X., Xu, K., Huang, L., Cao, F., & Song, Y. (2023). The Experimental Study of an R744 Heat Pump System for an Electric Vehicle for Cabin Cooling or Heating and Battery Fast Charging Cooling. *Energies*, 16(4), 2061. Doi: 10.3390/en16042061
- [23]. Savvakis, S., Dimopoulou, G., & Zoumpourlos, K. (2023). The Effect of the Isolator Design on the Efficiency of Rotary Piston Compressors. *Thermo*, 3(2), 216-231. Doi: 10.3390/thermo3020013.
- [24]. Almutairi, H. H., Almutairi, A. S., Suleiman, S. M., Alenezi, A. H., Alkhulaifi, K. A., & Alhajeri, H. M. (2023). Economic, Exergoeconomic and Exergoenvironmental Evaluation of Gas Cycle Power Plant Based on Different Compressor Configurations. *Processes*, 11(4), 1023. Doi: 10.3390/pr11041023
- [25]. Chandra, A. R., & Arora, R. C. (2012). *Refrigeration and air conditioning*. PHI Learning Pvt. Ltd..
- [26]. Awan, U. K. (2012). *Experimental Analysis of Variable Capacity Heat Pump System Equipped with Vapour Injection and Permanent Magnet Motor*. [Masters of Science Thesis, Royal Institute of Technology, KTH].
- [27]. Pezzutto, S., Grilli, G., & Zambotti, S. (2017). European heat pump market analysis: assessment of barriers and drivers. *International Journal of Contemporary ENERGY*, 3, 62-70.
- [28]. Hewitt, N. J. (2012). Heat pumps and energy storage—The challenges of implementation. *Applied Energy*, 89(1), 37-44.
- [29]. Genbach, A. A., Bondartsev, D. Y., & Iliev, I. K. (2018). Investigation of a high-forced cooling system for the elements of heat power installations. *Journal of machine Engineering*, 18. Doi: 10.5604/01.3001.0012.0937.
- [30]. Garaz, T. V., Ponomareva, YU. N., & Timoshenko, M. V. (2010). Chislavye kharakteristiki raspredeleniya pri obrabotke rezul'tatov eksperimenta. [Numerical distribution characteristics when processing experimental results]. *Elektrotekhnicheskiye i informatsionnyye komplekсы i sistemy*, 6(2), 42-45.
- [31]. Kornivets, D. (2009). Sistema CIC dlya porshnevnykh kompressorov «Bittser». [CIC system for Bitzer piston compressors]. *Kholodil'naya tekhnika*, (9), 4-8.
- [32]. Jiang, Y., Ma, Y., Li, M., & Fu, L. (2013). An experimental study of trans-critical CO₂ water–water heat pump using compact tube-in-tube heat exchangers. *Energy conversion and management*, 76, 92-100.
- [33]. Däwren, O.R. et al. (2015). *Teplovoy nasos*. [Heat pump]. Baza patentov Kazakhstana. Retrieved from: <https://kzpatents.com/4-ip30004-teplovoyj-nasos.html> [accessed: 25 June 2023].
- [34]. Kunelbayev, M., Omarov, R., Kurt, E., & Omar, D. (2021). Analysis of Energy and Exergy of a Two-Circuit Solar Installation with Thermosiphon Circulation. *WSEAS Transactions on Environment and Development*, 17, 1191-1200.
- [35]. *Programmable Resolution 1-Wire Digital Thermometer*. (2019). Maxim Integrated Products. Retrieved from: <https://www.analog.com/media/en/technical-documentation/data-sheets/DS18B20.pdf> [accessed: 27 June 2023].
- [36]. Montgomery, R., & McDowall, R. (2008). *Fundamentals of HVAC control systems*. Elsevier.
- [37]. *8-bit Atmel Microcontroller with 16/32/64KB In-System Programmable Flash*, Atmel. (2014). Atmel. Retrieved from: https://datasheet.lcsc.com/szlcsc/Microchip-Tech-ATMEGA644PA-AU_C38349.pdf [accessed: 03 July 2023].